

Excited State Magnetic Exchange Interactions Enable Large Spin Polarization Effects

Benjamin W. Stein,^{†,‡,§} Christopher R. Tichnell,[§] Ju Chen,[†] David A. Shultz,^{*,§,§} and Martin L. Kirk^{*,†,§}

[†]Department of Chemistry and Chemical Biology, The University of New Mexico, MSC03 2060, 1 University of New Mexico, Albuquerque, New Mexico 87131-0001, United States

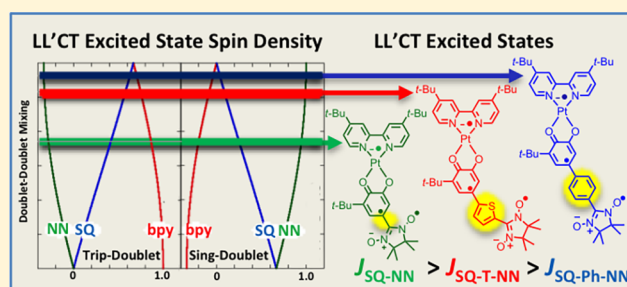
[‡]Chemistry Division, Los Alamos National Laboratory, Los Alamos, New Mexico 87545, United States

[§]Department of Chemistry, North Carolina State University, Raleigh, North Carolina 27695-8204, United States

Supporting Information

ABSTRACT: Excited state processes involving multiple electron spin centers are crucial elements for both spintronics and quantum information processing. Herein, we describe an addressable excited state mechanism for precise control of electron spin polarization. This mechanism derives from excited state magnetic exchange couplings that occur between the electron spins of a photogenerated electron–hole pair and that of an organic radical. The process is initiated by absorption of a photon followed by ultrafast relaxation within the excited state spin manifold. This leads to dramatic changes in spin polarization between excited states of the same multiplicity.

Moreover, this photoinitiated spin polarization process can be “read” spectroscopically using a magneto-optical technique that is sensitive to the excited state electron spin polarizations and allows for the evaluation of wave functions that give rise to these polarizations. This system is unique in that it requires neither intersystem crossing nor magnetic resonance techniques to create dynamic spin-polarization effects in molecules.



INTRODUCTION

The control and manipulation of dynamic spin processes in multispin molecular excited states is critical to developing large spin polarization effects^{1–4} for molecular spintronics^{5–8} and for engineering entangled spin systems for use in molecular quantum information processing technologies.^{9–12} A key goal toward understanding electronic structure contributions that govern dynamic excited state spin processes focuses on the nature of the photoexcited states involved and the interactions between multiple spin centers that are defined by pairwise magnetic exchange interactions (J_i). Magnetostructural correlations,^{13–16} where the exchange interaction is directly related to a structural parameter, have greatly impacted our understanding of electronic structure contributions to J_i ^{17–22} in the ground state and guided fields ranging from bioinorganic chemistry^{23,24} to molecular magnetism.^{25,26} In marked contrast, there exists a dearth of excited state magnetostructural correlations, particularly in cases where multiple exchange interactions are present. This has prompted us to design new molecular systems where photoexcitation generates excited states with multiple spin centers that are exchange coupled to one another. This allows for correlations to be developed between excited state J values and the underpinning geometric and electronic structure of the molecule, as well as the nature of excited state spin polarizations, dynamics, and lifetimes.

One strategy for designing such a tractable system is to covalently attach a spin center (e.g., an organic radical) to a

closed shell donor–acceptor chromophore. Upon photoexcitation, the open shell singlet nature of the chromophore results in the emergence of excited state J_i between the localized chromophore spins, which constitute the chromophore’s excited singlet (S) and triplet (T) states, and the spin localized on the organic radical. Thus, the radical spin center can function to admix components of the chromophore S and T states via the excited state exchange couplings. This has the potential to control entanglement of spins, and facilitate large spin polarization effects without the need for intersystem crossing.^{1,2,4,11,12} Importantly, the new J_i that result from appending an additional spin to a chromophore play a critical role in modulating excited state spin dynamics, resulting in a strategy for exerting wave function control over excited state lifetimes.^{1,2,4,27–29} Although molecular electron and nuclear spin manipulations may be controlled using pulsed NMR and EPR techniques,^{30,31} our focus here is on spin manipulation via excited state magnetic exchange interactions.

Herein, we present a series of molecules (Figure 1) that conclusively demonstrate the manipulation of excited state wave functions and spin polarizations by variation of the pairwise magnetic exchange interaction between a stable radical and one of the spins that derive from the open shell nature of the excited state donor–acceptor dyad.

Received: October 30, 2017

Published: February 5, 2018

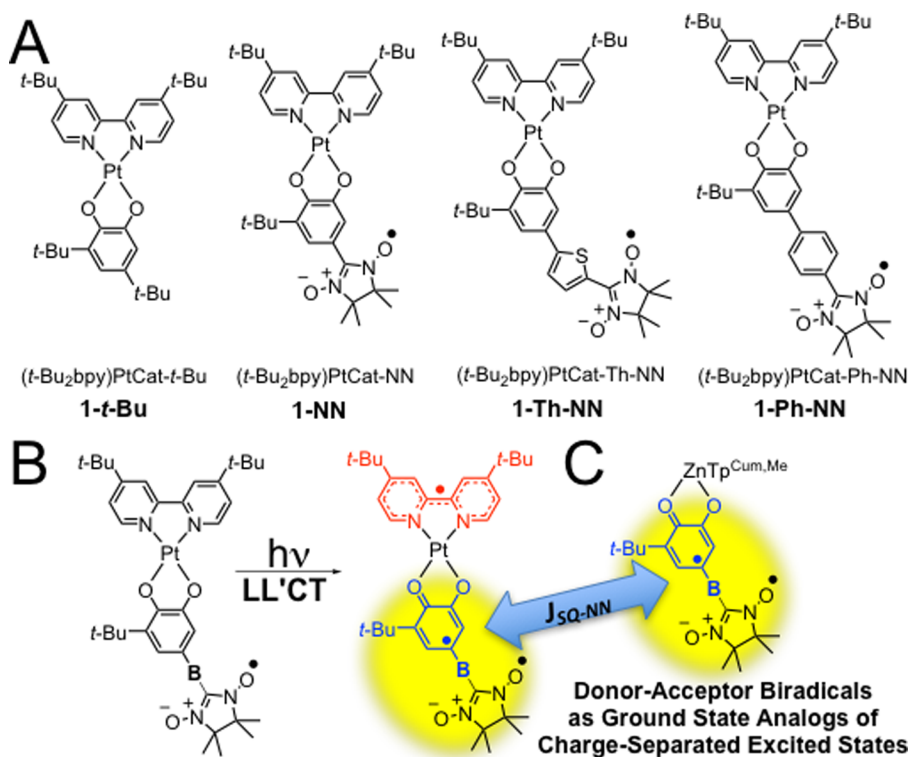


Figure 1. (A) Bond line drawings for the structures of the parent and radical-elaborated (*t*-Bu₂bpy)Pt(Cat-R) complexes. The *tert*-butyl groups on the bipyridine ligand are used to increase solubility and inhibit aggregation. As these *tert*-butyl groups have a negligible effect on the spectroscopy and electronic structure of our complexes, they are ignored in the discussion. (B) Photoinduced ligand-to-ligand charge transfer (LL'CT) resulting in semiquinone (SQ; hole) and bipyridine (bpy; electron) radicals. (C) Ground state donor–acceptor biradicals comprised of SQ and nitronyl nitroxide (NN) radicals serve as ground-state analogs of the donor half of the LL'CT excited states in B. ZnTp^{Cum,Me} = zinc(II) hydro-tris(3-cumenyl-5-methylpyrazolyl)borate. Ground state exchange couplings between SQ and NN radicals approximates the corresponding magnetic exchange couplings in the LL'CT excited states of **1-NN**, **1-Th-NN**, and **1-Ph-NN** and are used to derive LL'CT excited state energies and wave functions, see text.

RESULTS AND DISCUSSION

Electronic Absorption Spectra and Molecular Orbital Description of the Chromophores. The electronic absorption spectra for (*t*-Bu₂bpy)Pt(Cat-R), **1-*t*-Bu**, and three radical-elaborated complexes of the structural motif (*t*-Bu₂bpy)Pt(Cat-R), where R = NN (**1-NN**), 2,5-thiophene-NN (**1-Th-NN**), *para*-phenyl-NN (**1-Ph-NN**) and Cat = 3-*tert*-butyl-*ortho*-catecholate and NN = nitronyl nitroxide radical ($S = 1/2$), are displayed in Figure 2. A broad, featureless ligand-to-

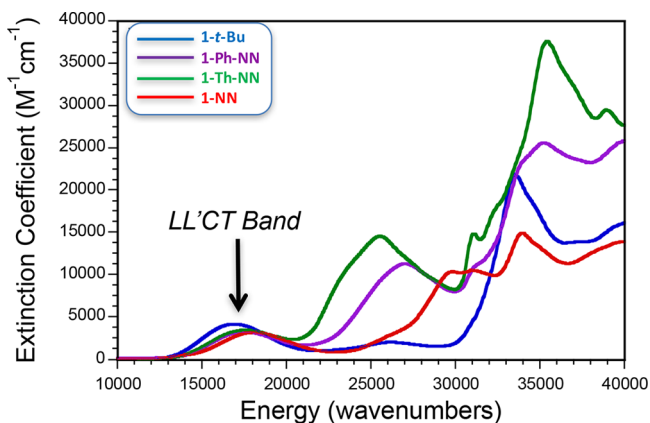


Figure 2. Electronic absorption spectra for **1-NN**, **1-Th-NN**, and **1-Ph-NN** recorded as solutions in methylene chloride.

ligand charge transfer^{32–34} (Cat → bpy LL'CT) band is observed at $\sim 16\,000\text{ cm}^{-1}$ in the low energy region of these electronic absorption spectra. This relatively intense Cat → bpy LL'CT band obscures a localized NN radical based transition (viz. NN(SOMO) → Ph-NN(LUMO)–Ph-NN(HOMO) → NN(SOMO)), which possesses a low oscillator strength in the $16\,000\text{--}18\,000\text{ cm}^{-1}$ region of the spectra of **1-NN**, **1-Th-NN**, and **1-Ph-NN**.³⁵ Neither the pendant NN radical spin nor the nature of the bridge (Ph or Th) in these (*t*-Bu₂bpy)Pt(Cat-R) chromophores result in dramatic changes to the LL'CT band relative to the nonradical elaborated **1-*t*-Bu**. The **1-*t*-Bu** parent molecule is only slightly red-shifted ($\sim 1000\text{ cm}^{-1}$) relative to the radical-elaborated species, and this principally derives from the electron withdrawing nature of the NN moiety.

Figure 3A,B shows the frontier orbitals that contribute to the observed LL'CT excitations in **1-*t*-Bu** and the radical-elaborated complexes, respectively. The NN SOMO is absent in the molecular orbital scheme for the **1-*t*-Bu** parent complex, and this leads to a diamagnetic $|S_0\rangle$ singlet ground state configuration for **1-*t*-Bu**. Thus, a one-electron promotion from the Cat HOMO to the bpy LUMO in **1-*t*-Bu** results in both singlet, $|S_1\rangle$, and triplet, $|T_1\rangle$, charge-separated, biradical excited states with the hole localized primarily on the Cat donor (viz. a SQ radical) and the promoted electron localized predominantly on the bpy acceptor.³² The Cat-bpy chromophore components of these configurations are depicted within the color-coded boxes of Figure 3C. The nature of this LL'CT transition has been evaluated using time-dependent density functional theory

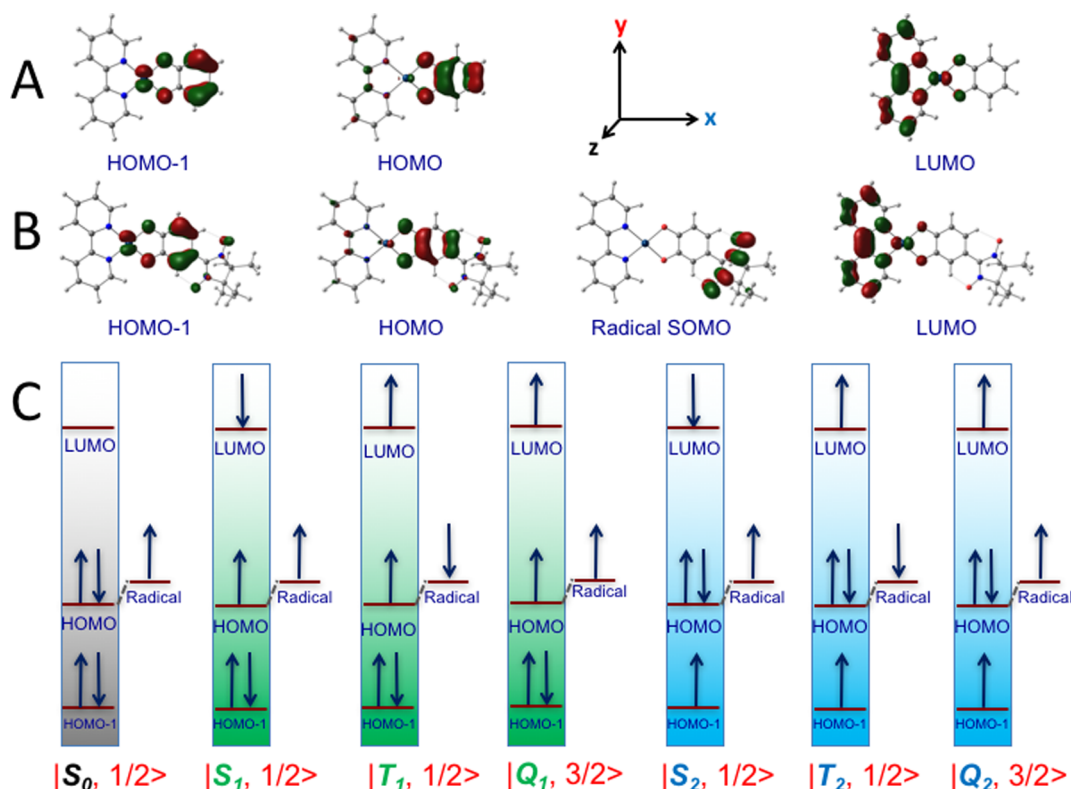


Figure 3. Frontier Kohn–Sham molecular orbitals for **1-*t*-Bu** (A) and **1-NN** (B). (C) Excited state configurations derived from one-electron promotions from the HOMO and HOMO–1 to the LUMO for **1-*t*-Bu** (colored-coded boxes) and for radical-elaborated (*t*-Bu₂bpy)Pt(Cat-R) complexes. Molecular orbitals for **1-*t*-Bu** (A) are plotted with an isovalue of 0.05 e/Å³, and those for **1-NN** are plotted with an isovalue of 0.06 e/Å³.

(TD-DFT), and the analysis indicates that the LL′CT transition is ~99% HOMO → LUMO (CAT → bpy) in nature with only a minor contribution from the Pt center.³² The $S_0 \rightarrow S_1$ transition in **1-*t*-Bu** is spin-allowed, while the $S_0 \rightarrow T_1$ transition is spin-forbidden. A similar manifold of excited states is present at higher energy. These states are generated from one-electron promotions originating on the Cat HOMO–1 to the bpy LUMO, and these $|S_2\rangle$ and $|T_2\rangle$ excited states are polarized along the short, in-plane axis, perpendicular to the x -polarized $S_0 \rightarrow S_1$ and $S_0 \rightarrow T_1$ transitions.³² Accurate assignments of the $S_0 \rightarrow S_2$ and $S_0 \rightarrow T_2$ transitions are complicated by the spin-forbidden nature of the latter, and the fact that the $S_0 \rightarrow S_2$ transition possesses a weaker oscillator strength since it is polarized along the short axis of the molecule, perpendicular to the charge transfer direction.

As mentioned above, appending a persistent NN radical to **1-*t*-Bu** results in the appearance of the localized NN radical SOMO in the molecular orbital scheme, Figure 3B. This does not change the gross orbital parentage of the one-electron promotions that contribute to the LL′CT transitions observed in **1-NN**, **1-Th-NN**, and **1-Ph-NN**. However, in contrast to **1-*t*-Bu**, when the NN-elaborated complexes are optically excited to their low-energy Cat → bpy LL′CT excited states the near quantitative charge transfer³² yields triradical (bpy•)Pt(SQ•-NN•) charge and spin distributions (Figures 1B and 3C). There are now two dominant pairwise exchange interactions in the 3-spin LL′CT excited states for **1-NN**, **1-Th-NN**, and **1-Ph-NN**, and the nature of these excited state exchange interactions are discussed below.

Excited State Exchange Interactions. When the NN radical spin is appended to the **1-*t*-Bu** chromophore, the ground state changes from $S_T = 0$ to an $S_T = 1/2$ spin doublet, |

$S_0, 1/2\rangle$. The S_0 in the $|S_0, 1/2\rangle$ function for (*t*-Bu₂bpy)Pt(Cat-R) indicates the ground state spin singlet nature of the (*t*-Bu₂bpy)Pt(Cat) chromophore and the “1/2” indicates the total spin of the system (Figure 3C). This results in a more complex excited state spin manifold relative to the $|S_i\rangle$ and $|T_i\rangle$ states of **1-*t*-Bu**. The new excited state manifolds are now described in terms of spin-quartet $|T_i, 3/2\rangle$, and spin-doublet $|T_i, 1/2\rangle$ and $|S_i, 1/2\rangle$ excited states due to the exchange interaction between the $S = 1/2$ NN radical spin center and the S_i and T_i excited states of the chromophore (Figure 3C), respectively. Thus, we may now take advantage of the spin-Hamiltonian formalism to determine the energy levels of the $|T_i, 3/2\rangle$, $|T_i, 1/2\rangle$, and $|S_i, 1/2\rangle$ excited states in terms of the magnetic exchange interactions between the individual SQ•, bpy•, and NN• spin centers. These energy splittings are defined by the pairwise exchange Hamiltonian for a linear triad in eq 1. This approach will also allow for the determination of excited state wave functions, spin populations, and spin polarization effects.

$$H_{\text{ex}} = -2J_{\text{SQ-bpy}}(\hat{S}_{\text{SQ}} \cdot \hat{S}_{\text{bpy}}) - 2J_{\text{SQ-NN}}(\hat{S}_{\text{SQ}} \cdot \hat{S}_{\text{NN}}) \quad (1)$$

Here, the J_i are the excited state pairwise exchange interactions between the three spin centers, SQ, bpy•, and NN (the “•” on SQ and NN and *t*-Bu₂ on bpy have been omitted for brevity), in the (bpy)Pt(Cat-R) complexes, which can be evaluated using experimental data as described below. The paramagnetic **1-NN**, **1-Th-NN**, and **1-Ph-NN** complexes are all linear spin triads in the LL′CT excited state with no direct NN-bpy connectivity. Therefore, the far weaker $J_{\text{NN-bpy}}$ exchange interaction can be ingored in the analysis of the data.^{13,36–38}

Since the LL′CT excited state of each complex is characterized by a unit charge transfer, and J varies linearly

with spin densities, $J_{\text{SQ-bpy}}$ will be constant in this series.^{18,39–42} This is reflected in the similarity of the MCD spectra for the series, where the interdoublet splitting is dominated by the magnitude of $J_{\text{SQ-bpy}}$. Thus, the $J_{\text{SQ-NN}}$ -dependent $|S_{i,1/2}\rangle$, $|T_{i,1/2}\rangle$, and $|T_{i,3/2}\rangle$ energies are plotted in Figure 4 using a

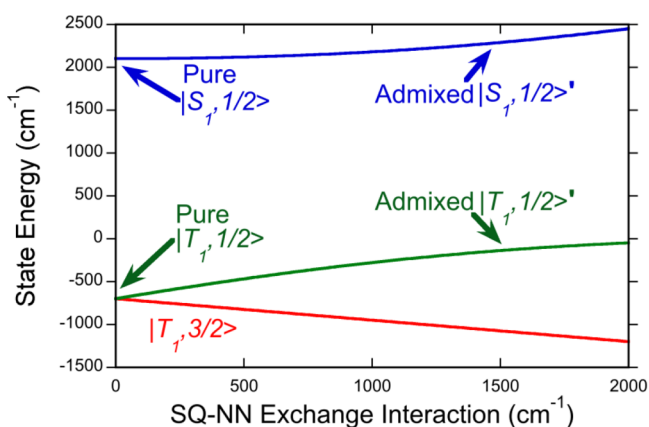


Figure 4. State energy diagram for $|S_{i,1/2}\rangle$, $|T_{i,1/2}\rangle$, and quartet excited states in (*t*-Bu₂bpy)Pt(Cat-R) chromophores as a function of the excited state SQ-NN exchange interaction, $J_{\text{SQ-NN}}$ with fixed $J_{\text{SQ-bpy}} = 1400 \text{ cm}^{-1}$. Note the curvature that results from exchange dependent $|S_{i,1/2}\rangle - |T_{i,1/2}\rangle$ mixing (i.e., λ in eq 4).

constant $J_{\text{SQ-bpy}} = 1400 \text{ cm}^{-1}$ (*vide infra*). The exchange-dependent mixing of the $|S_{i,1/2}\rangle$ and $|T_{i,1/2}\rangle$ doublet states are an interesting consequence of a linear triad of spins with two unequal, pairwise exchange interactions⁴³ as described by eq 1.²⁶ In this general case, the $|T_{i,1/2}\rangle$ and $|S_{i,1/2}\rangle$ states with the same $S_T = 1/2$ total spin can mix with one another via an off-diagonal matrix element in the exchange Hamiltonian.^{26,44} This is important, since it means that the magnetic exchange interaction (J_i) between an electron spin and a photogenerated electron–hole pair can facilitate a localized intersystem crossing ($|S_{i,1/2}\rangle \rightarrow |T_{i,1/2}\rangle$) between the chromophore LL'CT S_i and T_i excited states.^{1,2,29,45}

The magnitude of the $|S_{i,1/2}\rangle$ and $|T_{i,1/2}\rangle$ excited state wave function mixing can be parametrized by λ ,^{44,46} and this quantifies the amount of $|T_{i,1/2}\rangle$ ($|S_{i,1/2}\rangle$) character admixed into the $|S_{i,1/2}\rangle$ ($|T_{i,1/2}\rangle$) wave function by the $J_{\text{SQ-NN}}$ exchange interaction according to

$$\left| S_{i, \frac{1}{2}} \right\rangle' = \cos \lambda \left| S_{i, \frac{1}{2}} \right\rangle - \sin \lambda \left| T_{i, \frac{1}{2}} \right\rangle \quad (2)$$

$$\left| T_{i, \frac{1}{2}} \right\rangle' = \cos \lambda \left| T_{i, \frac{1}{2}} \right\rangle + \sin \lambda \left| S_{i, \frac{1}{2}} \right\rangle \quad (3)$$

where the primed functions indicate exchange-admixed states (see also Figure 4). Thus, knowledge of the individual $J_{\text{SQ-NN}}$ and $J_{\text{SQ-bpy}}$ pairwise exchange interactions (*vide infra*) allows us to determine the value of λ , and the mixing coefficient, $\sin \lambda$, for each of our radical-elaborated chromophores according to eq 4:⁴⁴

$$\lambda = \frac{1}{2} \tan^{-1} \frac{\sqrt{3} J_{\text{SQ-NN}}}{2 J_{\text{SQ-bpy}} - J_{\text{SQ-NN}}} \quad (4)$$

yielding the excited state admixed wave functions ($|S_{i,1/2}\rangle'$ and $|T_{i,1/2}\rangle'$) directly from experimental observables. The $J_{\text{SQ-NN}}$ exchange values are known with high accuracy from ground

state magnetic susceptibility measurements,¹⁹ and the $J_{\text{SQ-bpy}}$ value is determined using magnetic circular dichroism (MCD) spectroscopy.

Magnetic Circular Dichroism Spectroscopy. Both the S_1 and T_1 LL'CT excited states of **1-*t*-Bu** possess A_1 symmetry at the local C_{2v} symmetry of the Pt site (Figure 3A). As such, there is no spin orbit matrix element that connects these two states and $\langle T_1 | L_i | S_1 \rangle = 0$ (the L_i transform as a_2 , b_1 , and b_2 in C_{2v}). Thus, conversion of the S_1 state to the T_1 state by intersystem crossing (ISC) is forbidden, and fast nonradiative relaxation back to the S_0 ground state is observed.³² In contrast, spin orbit mixing of the low energy S_1 and T_1 (1A_1 and 3A_1) states with the higher energy T_2 and S_2 (3B_1 and 1B_1) states is symmetry allowed.³² In fact, the presence of $|S_{i,1/2}\rangle - |T_{i,1/2}\rangle$ wave function mixing, the paramagnetic nature of the ground states, and Pt-induced excited state spin orbit (SOC) “switches on” an exchange-dependent magneto-optical activity in these radical-elaborated complexes, which can be probed exclusively and at high resolution by MCD spectroscopy. A pictorial mechanism for the observed dependence of MCD activity on λ is summarized in Figure 5.^{47,48}

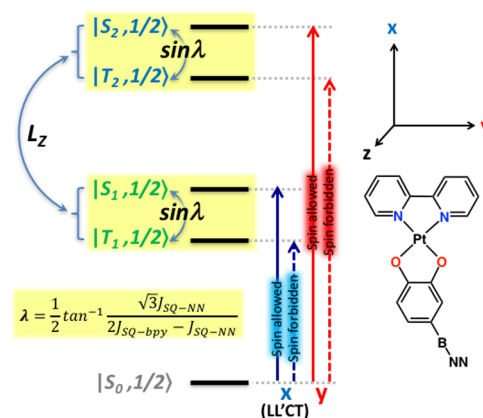


Figure 5. Mechanism for MCD activity in **1-NN**, **1-Th-NN**, and **1-Ph-NN**. MCD activity entails two orthogonal transition dipoles (x - and y -polarized HOMO \rightarrow LUMO and HOMO–1 \rightarrow LUMO, respectively) that are mixed by the spin–orbit operator $\pm L_z$. Solid vertical arrows indicate spin-allowed transitions and dashed arrows indicate spin-forbidden excitations. The latter gain intensity due to interdoublet exchange mixing ($\propto \sin \lambda$, eqs 2 and 3 and Table 1) between the $|T_{i,1/2}\rangle$ and $|S_{i,1/2}\rangle$ configurations, as well as between the two higher energy $|T_{i,1/2}\rangle$ and $|S_{i,1/2}\rangle$ configurations. This is important as it relaxes the spin selection rule and allows for the onset of C-term MCD activity.

No temperature-dependent C-term MCD is observed for diamagnetic chromophores like the **1-*t*-Bu** parent complex since a paramagnetic ground state is required.^{47,48} Furthermore, C-term MCD is not expected for organic radicals like the catechol-bridge-NN ligands due to the small SOC constants of the constituent atomic centers.^{47,48} In contrast, C-term MCD signals for radical elaborated **1-NN**, **1-Th-NN**, and **1-Ph-NN** are observed and the corresponding spectra are presented in Figure 6. Thus, the incorporation of a pendant, persistent radical to the (*t*-Bu₂bpy)Pt(Cat) chromophore imparts magneto-optical activity in **1-NN**, **1-Th-NN**, and **1-Ph-NN** with a magnitude that is both temperature- and bridge-dependent. Although only one LL'CT transition ($|S_0\rangle \rightarrow |T_1\rangle$) is observed in the electronic absorption spectrum of **1-*t*-Bu**, two MCD bands are observed in this LL'CT region for radical-

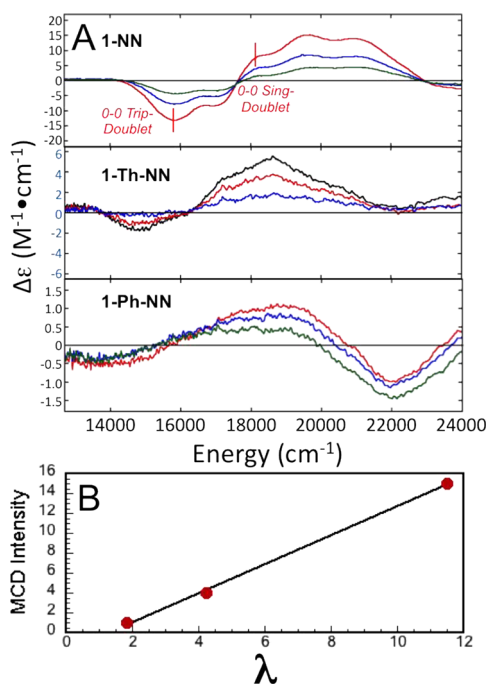


Figure 6. (A) Variable temperature (2.5 K, black; 5 K, red; 10 K, blue; 20 K, green) magnetic circular dichroism (VT-MCD) spectra of complexes **1-NN**, **1-Th-NN**, and **1-Ph-NN**. (B) Apparent linear dependence of the MCD intensity on λ , from eq 4.

elaborated **1-NN**, **1-Th-NN**, and **1-Ph-NN**. We assign the higher-energy of these two MCD bands as the spin-allowed $|S_0,1/2\rangle \rightarrow |S_1,1/2\rangle$ transition and the lower energy MCD band as the $|S_0,1/2\rangle \rightarrow |T_1,1/2\rangle$ transition within the lowest energy LL'CT manifold (Figures 3C and 5). The assignment of these two, low-energy MCD bands as arising from excited states with the same orbital parentage is supported by their relative energies with respect to the LL'CT band in the electronic absorption spectra, and the fact that the vibronic progressions observed for the $|S_0,1/2\rangle \rightarrow |T_1,1/2\rangle$ and $|S_0,1/2\rangle \rightarrow |S_1,1/2\rangle$ transitions ($0-0$ to $0-1 = 1276 \text{ cm}^{-1}$) are identical and are thus built upon the same progression forming mode.

The magnitude of the $J_{\text{SQ-bpy}}$ exchange interaction can be directly addressed from the low-temperature MCD spectra presented in Figure 6, where both the $|S_0,1/2\rangle \rightarrow |S_1,1/2\rangle$, and $|S_0,1/2\rangle \rightarrow |T_1,1/2\rangle$ transitions that possess Cat \rightarrow bpy LL'CT character are observed. The pure electronic $0-0$ transitions at $18\,300 \text{ cm}^{-1}$ ($|S_1,1/2\rangle$) and $15\,800 \text{ cm}^{-1}$ ($|T_1,1/2\rangle$) are clearly present in the **1-NN** spectra and less so in the **1-Th-NN** spectra. This allows $J_{\text{SQ-bpy}}$ to be estimated from the energy difference between the $|S_0,1/2\rangle \rightarrow |S_1,1/2\rangle$, and $|S_0,1/2\rangle \rightarrow |T_1,1/2\rangle$ $0-0$ transitions ($2J_{\text{SQ-bpy}} \approx 2500 \text{ cm}^{-1}$). As mentioned previously and depicted in Figure 1C, the excited state $J_{\text{SQ-NN}}$ values detailed in eq 1 can be approximated by the corresponding ground-state biradical $J_{\text{SQ-NN}}$ values. These $J_{\text{SQ-NN}}$ values (Table 1) have been determined from magnetic susceptibility measurements on $\text{Tp}^{\text{Cum,Me}}\text{Zn}(\text{SQ-bridge-NN})$ complexes that possess the same charge/spin distributions and the same bridge fragments as is found in the lowest energy LL'CT excited states of **1-NN**, **1-Th-NN**, and **1-Ph-NN**: $\text{Tp}^{\text{Cum,Me}}\text{Zn}(\text{SQ-NN})$ ($J_{\text{SQ-NN}} = +550 \text{ cm}^{-1}$), $\text{Tp}^{\text{Cum,Me}}\text{Zn}(\text{SQ-Th-NN})$ ($J_{\text{SQ-NN}} = +200 \text{ cm}^{-1}$),¹⁹ and $\text{Tp}^{\text{Cum,Me}}\text{Zn}(\text{SQ-Ph-NN})$ ($J_{\text{SQ-NN}} = +100 \text{ cm}^{-1}$).^{19,40}

Table 1. Exchange Parameters and Mixing Coefficients for Radical-Elaborated (*t*-Bu₂bpy)Pt(Cat-R) Complexes

complex	$J_{\text{SQ-bpy}}$ (cm^{-1}) ^a	$J_{\text{SQ-NN}}$ (cm^{-1}) ^b	λ ^c	$\sin \lambda$ ^d
1-NN	+1400	+550	11.5	0.199
1-Th-NN	+1400	+220	4.25	0.074
1-Ph-NN	+1400	+100	1.83	0.032

^a $J_{\text{SQ-bpy}}$ exchange parameter determined iteratively using the $|S_1,1/2\rangle' - |T_1,1/2\rangle'$ energy gap from the MCD spectrum of **1-NN**. ^b $J_{\text{SQ-NN}}$ exchange parameter assumed to be equivalent to ground state biradicals shown in Figure 1C. ^c λ calculated using eq 4 and experimental J values. ^dThe value of $\sin \lambda$ provides the amount of $|T_1,1/2\rangle$ ($|S_1,1/2\rangle$) mixed into $|S_1,1/2\rangle$ ($|T_1,1/2\rangle$) as per eqs 2 and 3.

The $J_{\text{SQ-NN}}$ -dependent $|S_1,1/2\rangle$, $|T_1,1/2\rangle$, and $|T_1,3/2\rangle$ state energies that were given in Figure 4 utilize the experimentally observed energy gap between the $0-0$ transitions associated with $|S_0,1/2\rangle \rightarrow |S_1,1/2\rangle$ and $|S_0,1/2\rangle \rightarrow |T_1,1/2\rangle$ transitions in **1-NN** as a starting point to iteratively determine the value of $J_{\text{SQ-bpy}}$ (1400 cm^{-1} , Table 1) as $J_{\text{SQ-NN}} \rightarrow 0 \text{ cm}^{-1}$. Thus, a $2J_{\text{SQ-bpy}}$ splitting of 2800 cm^{-1} is determined to be the intrinsic excited state $|S_1\rangle - |T_1\rangle$ singlet–triplet gap for the parent complex, **1-*t*-Bu**. Furthermore, using the experimentally determined $J_{\text{SQ-NN}}$ and $J_{\text{SQ-bpy}}$ values in the context of eq 4 allows us to determine λ which varies from 11.5 for **1-NN** to 1.83 for **1-Ph-NN** (see Table 1). In the present case, $J_{\text{SQ-bpy}}$ is effectively a constant, while $J_{\text{SQ-NN}}$ is an exchange-modified variable (Figure 4 and Table 1). Our experimentally determined values for $J_{\text{SQ-bpy}}$ and $J_{\text{SQ-NN}}$, when evaluated in the context of eq 1, allow us to demonstrate the effects of $J_{\text{SQ-NN}}$ modulation on the $|S_1,1/2\rangle'$ and $|T_1,1/2\rangle$ spin eigenfunctions, as well as the degree of excited state spin polarization in these radical-elaborated complexes. The details of these exchange modulated excited state spin polarizations are discussed in detail below.

Implication for Spin Polarization Effects as a Function of Radical-Chromophore Exchange. Figure 7 shows the excited doublet net spin populations on the NN, SQ, and bpy centers (green, blue, and red, respectively, in Figure 7) that are calculated by applying a Heitler–London approach^{26,49} using experimentally determined pairwise exchange parameters within the Heisenberg–Dirac–Van Vleck (HDVV) formalism as detailed by Kahn.²⁶ Importantly, the spin populations localized on the NN, SQ, and bpy centers are determined by the magnitude of the interdoubt state mixing parameter, λ .⁴⁴ In the absence of a $J_{\text{SQ-NN}}$ exchange interaction, the spin density of the SQ-bpy LL'CT dyad singlet state is zero and the MCD intensity is also zero. The magnitude of $J_{\text{SQ-NN}}$ modulates the excited state doublet wave function mixing, altering the SQ-bpy spin density distribution, and the MCD intensity is found to vary linearly with λ , Figure 6B. This plot of MCD intensity vs λ clearly shows that $I_{\text{MCD}} \rightarrow 0$ as $\lambda \rightarrow 0$, indicating that there will be no spin population on the chromophoric SQ or bpy sites in the $|S_1,1/2\rangle$ wave function in the absence of exchange-mediated mixing with the $|T_1,1/2\rangle$ state.⁴⁶

Optical excitation from the $|S_0,1/2\rangle$ ground state to $|S_1,1/2\rangle'$ in **1-NN**, **1-Th-NN**, and **1-Ph-NN** results in an exchange-dependent net spin population transfer from NN (100% in the electronic ground state) to SQ and bpy in the $|S_1,1/2\rangle'$ excited state. The $J_{\text{SQ-NN}}$ excited state exchange interaction that allows the $|S_1,1/2\rangle$ and $|T_1,1/2\rangle$ states to mix with one another also provides a novel mechanism for a highly efficient $|S_1,1/2\rangle' \rightarrow |T_1,1/2\rangle'$ internal conversion (IC) process. Population of the

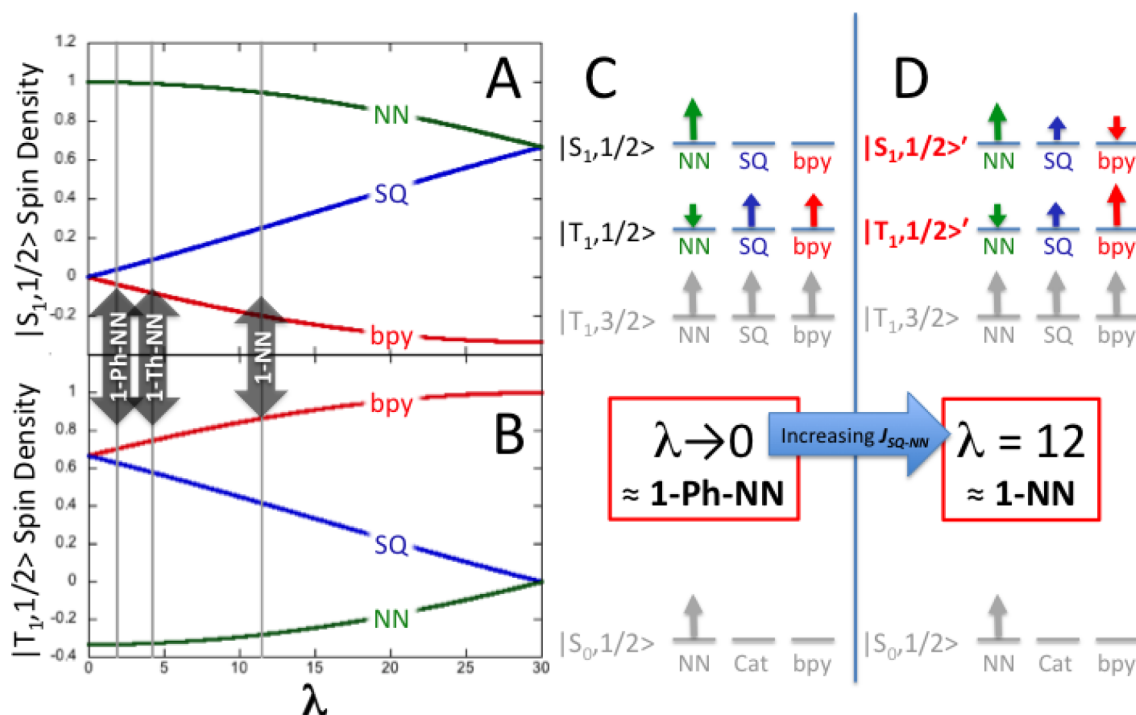


Figure 7. $|S_{1,1/2}\rangle$ (A) and $|T_{1,1/2}\rangle$ (B) spin populations for the three spin centers (bpy•, SQ and NN, color-coded to match C and D) as a function of λ . Gray vertical lines indicate “experimental” values of λ for 1-Ph-NN (1.83), 1-Th-NN (4.25), and 1-NN (11.5) that are approximated by the spin density illustrations in panels C and D. (C and D) Graphical depictions of J_{SQ-NN} -modulated excited state spin populations on NN, SQ, and bpy for $\lambda \rightarrow 0$ (\approx weak J_{SQ-NN} ; C) and for $\lambda = 12$ (\approx strong J_{SQ-NN} ; D) in radical elaborated (*t*-Bu₂bpy)Pt(Cat-R) complexes.

$|T_{1,1/2}'\rangle$ state by IC or by direct photoexcitation will result in a marked change in the spin populations on the NN, SQ, and bpy• centers relative to the $|S_{1,1/2}'\rangle$ state. Namely, the NN- and bpy-centered spins flip during the $|S_{1,1/2}'\rangle \rightarrow |T_{1,1/2}'\rangle$ process and their relative magnitudes are reversed.

We note that both the magnitude and sign of these spin populations can be further controlled by the nature of the J_{SQ-NN} interaction through its effect on λ . Most importantly, the $|T_{1,1/2}'\rangle \rightarrow |T_{1,3/2}\rangle$ ISC is both spin- and symmetry-forbidden in these systems resulting in no net population of $|T_{1,3/2}\rangle$ and no observed $|T_{1,3/2}\rangle \rightarrow |S_{0,1/2}\rangle$ phosphorescence. Thus, a nonradiative $|T_{1,1/2}'\rangle \rightarrow |S_{0,1/2}\rangle$ IC process dominates repopulation of the $|S_{0,1/2}\rangle$ ground state. This $|T_{1,1/2}'\rangle \rightarrow |S_{0,1/2}\rangle$ relaxation causes the NN spin to flip again, with a concomitant temporal redistribution of the $|S_{0,+1/2}\rangle$ and $|S_{0,-1/2}\rangle$ ground state populations as Boltzmann equilibrium is reached. This also provides a mechanism for the ultrafast hyperpolarization of nuclear spins located on, or attached to, the bpy acceptor. The bpy acceptor nitrogen atoms are located ~ 8 Å from the NN bridgehead carbon, and are therefore remote from the spatial confinement of the ground state electron spin localized on the NN radical. Future experiments will probe hyperpolarization of the NN spin and critical $|T_{1,1/2}'\rangle \rightarrow |S_{0,1/2}\rangle$ relaxation processes, including the potential for magnetic exchange control of $|T_{1,1/2}'\rangle \rightarrow |S_{0,1/2}\rangle$ IC rates to repopulate the $|S_{0,1/2}\rangle$ ground state.

SUMMARY

We have developed a chromophoric spin system where each spin-1/2 subsystem in the tripartite excited doublet states is entangled with the remaining two spins, and we have probed the magneto-optical properties of these systems using variable-temperature MCD spectroscopy. The open-shell singlet nature

of the LL'CT charge separated state provides a convenient platform for facilitating strong pairwise excited state exchange coupling between the three spin centers (NN, SQ, and bpy•) in (*t*-Bu₂bpy)Pt(Cat-Bridge-NN). A critical magnetic exchange mixing is observed between the excited $|S_{1,1/2}\rangle$ and $|T_{1,1/2}\rangle$ wave functions, providing a means of accessing the “dark” T_1 triplet configuration of the bpy-Cat chromophore that is otherwise spectroscopically inaccessible in the nonradical elaborated 1-*t*-Bu parent complex. Moreover, the $|T_{1,1/2}'\rangle$ excited state wave function is shown to possess dramatically different NN, SQ, and bpy• spin populations relative to the ground ($|S_{0,1/2}\rangle$) and excited ($|S_{1,1/2}'\rangle$) doublet states, and these spin populations are controlled by the pairwise exchange interactions (J_{SQ-bpy} and J_{SQ-NN}) and the interdoublet mixing parameter, λ . Remarkably, the MCD intensity is found to be a linear function of λ , correlating magneto-optical activity with spin polarization effects. Thus, our results show that magnetic “exchange fields” generated by radical attachment to molecular chromophores can control the admixture of chromophore singlet and triplet states, modulate entanglement of remote spin centers, facilitate spin polarization transfer processes with high efficiency, and yield exchange dependent magneto-optical activity. Furthermore, this tripartite system can be generated on an ultrafast time scale via the spin-allowed $|S_{0,1/2}\rangle \rightarrow |S_{1,1/2}'\rangle$ photoexcitation process (Figures 1B and 3C) and can be modulated by well-defined synthetically accessible individual pairwise exchange interactions, which determine interstate mixing between exchange-coupled $|S_{1,1/2}\rangle$ and $|T_{1,1/2}\rangle$ states through λ .^{32,50}

EXPERIMENTAL SECTION

Synthesis. All synthetic procedures were carried out under a N₂ atmosphere and used reagents purified by standard literature

procedures. NN-CatH₂, NN-Ph-CatH₂, NN-Th-CatH₂, and (di-*tert*-butyl-bipyridine)PtCl₂ were synthesized by literature methods. 2-Methyltetrahydrofuran was purchased from Alfa Aesar and purified by passage down a column of basic alumina immediately before use. (Di-*tert*-butyl-bipyridine)Pt(Cat) compounds were synthesized by reaction of (di-*tert*-butyl-bipyridine)PtCl₂, protonated catechol ligand, and *tert*-BuOK in MeOH. Complexes 1-*t*-Bu, 1-NN, 1-Ph-NN, and 1-Th-NN were prepared using literature methods (see the Supporting Information, SI for synthetic details). The solution, room-temperature EPR spectra (see Figure S1 for spectra) of these NN-elaborated complexes are characteristic of an organic NN radical and display hyperfine splitting due to electron spin coupling to two equivalent $I = 1$ ¹⁴N nuclei. The isotropic EPR spectra possess spin-only g values ($g = 2.001$) with no evidence of hyperfine coupling to the ¹⁹⁵Pt nucleus ($I = 1/2$). These spectral characteristics derive from the fact that the NN singly occupied molecular orbital (SOMO) possesses a node at the carbon atom that is bonded to the Cat ring.^{18,41,51} This effectively limits both NN spin- and electron delocalization, and results in no Pt character being present in the NN SOMO and no measurable spin delocalization onto the Pt ion. Additional synthetic details and characterization are available in the SI.

MCD Spectroscopy. MCD spectra were collected on an Oxford SM4000T magneto-optical cryostat interfaced with a Jasco J-810 spectropolarimeter. Samples were made up as 2-methyltetrahydrofuran solutions and injected into a custom brass sample holder containing spectro-sil quartz windows, a butyl rubber spacer, and rubber o-rings. The samples were frozen in liquid N₂ and loaded into the MCD cryostat. Depolarization was checked by use of a nickel tartrate sample placed before and after the cryostat; samples that displayed less than 5% depolarization were deemed suitable. Baseline correction was performed by subtraction of a 0 T spectrum. Where necessary, B-term spectral contributions were eliminated by subtraction of a high-temperature (50 K), high-field (7 T) spectrum from the low-temperature spectra. Samples with very weak S/N were further enhanced by the collection of spectra in positive and negative applied magnetic fields. Spectral subtraction (positive - negative) then yields MCD spectra that are free of zero-field contributions.

EPR Spectroscopy. Fluid solution room temperature EPR spectra were collected on a Bruker EMX EPR spectrometer. Sample concentrations were ~0.1 mM in 2-methyltetrahydrofuran.

Electronic Absorption Spectroscopy. Electronic absorption spectra were taken on a Hitachi U-4100 double beam spectrophotometer. Room temperature samples were made up as 2-methyltetrahydrofuran solutions and loaded into a microvolume quartz cuvette. Low temperature absorption spectra were taken with a custom Janis liquid He flow cryostat mounted in a Hitachi U-3100 spectrophotometer. Samples were loaded into a brass sample holder identical to that used for MCD measurements, and baseline corrected with a frozen solvent sample. Temperature was monitored with a silicon diode and a Lakeshore temperature controller and was adjusted by changing the flow of liquid He through the cryostat and with a nichrome wire heater located above the sample.

Computational Methods. All calculations were performed with the ORCA 3.0.1 or 3.0.2 program suite.⁵² Density functional theory (DFT) calculations were performed using the def2-TZVP basis⁵³ and the PBE GGA functional.⁵⁴ CASSCF/NEVPT2^{55–58} calculations used quasi-restricted orbitals (QROs) from the DFT calculations as the initial guess orbitals. Minimal active space calculations (CAS(3,3) or CAS(2,2)) for radical elaborated or nonelaborated compounds, respectively) were first performed, and the molecular orbitals obtained were used for subsequent calculations using larger active spaces. All CASSCF calculations utilized the RIJCOSX approximation.⁵⁹

■ ASSOCIATED CONTENT

● Supporting Information

The Supporting Information is available free of charge on the ACS Publications website at DOI: 10.1021/jacs.7b11397.

Synthesis and characterization information. (PDF)

■ AUTHOR INFORMATION

Corresponding Authors

*shultz@ncsu.edu.

*mkirk@unm.edu.

ORCID

Benjamin W. Stein: 0000-0002-0366-5476

David A. Shultz: 0000-0001-8121-6812

Martin L. Kirk: 0000-0002-1479-3318

Notes

The authors declare no competing financial interest.

■ ACKNOWLEDGMENTS

M.L.K. acknowledges NSF CHE 1565930 and NSF Grant No. IIA-1301346 for financial support. D.A.S. acknowledges financial support from NSF (CHE-1464085). B.W.S. acknowledges the Los Alamos National Laboratory Glenn T. Seaborg Institute for a postdoctoral fellowship.

■ REFERENCES

- (1) Zarea, M.; Ratner, M. A.; Wasielewski, M. R. *J. Chem. Phys.* **2015**, *143*, 054101.
- (2) Matsumoto, T.; Teki, Y. *Phys. Chem. Chem. Phys.* **2012**, *14*, 10178.
- (3) Kanemoto, K.; Fukunaga, A.; Yasui, M.; Kosumi, D.; Hashimoto, H.; Tamekuni, H.; Kawahara, Y.; Takemoto, Y.; Takeuchi, J.; Miura, Y.; Teki, Y. *RSC Adv.* **2012**, *2*, 5150.
- (4) Teki, Y.; Tamekuni, H.; Haruta, K.; Takeuchi, J.; Miura, Y. *J. Mater. Chem.* **2008**, *18*, 381.
- (5) Wolf, S. A.; Awschalom, D. D.; Buhrman, R. A.; Daughton, J. M.; von Molnar, S.; Roukes, M. L.; Chtchelkanova, A. Y.; Treger, D. M. *Science* **2001**, *294*, 1488.
- (6) Shultz, D. A.; Kirk, M. L. *Chem. Commun.* **2014**, *50*, 7401.
- (7) Herrmann, C.; Elmsiz, J. *Chem. Commun.* **2013**, *49*, 10456.
- (8) Sanvito, S. *Chem. Soc. Rev.* **2011**, *40*, 3336.
- (9) Lehmann, J.; Gaita-Arino, A.; Coronado, E.; Loss, D. *J. Mater. Chem.* **2009**, *19*, 1672.
- (10) Stamp, P. C. E.; Gaita-Arino, A. *J. Mater. Chem.* **2009**, *19*, 1718.
- (11) Baart, T. A.; Fujita, T.; Reichl, C.; Wegscheider, W.; Vandersypen, L. M. K. *Nat. Nanotechnol.* **2016**, *12*, 26.
- (12) Amit Kumar, P.; Indrani, B. *J. Phys.: Condens. Matter* **2010**, *22*, 016004.
- (13) Kessissoglou, D. P.; Kirk, M. L.; Lah, M. S.; Li, X. H.; Raptopoulou, C.; Hatfield, W. E.; Pecoraro, V. L. *Inorg. Chem.* **1992**, *31*, 5424.
- (14) Crawford, V. H.; Richardson, H. W.; Wasson, J. R.; Hodgson, D. J.; Hatfield, W. E. *Inorg. Chem.* **1976**, *15*, 2107.
- (15) Scaringe, R. P.; Hodgson, D. J.; Hatfield, W. E. *Transition Met. Chem.* **1981**, *6*, 340.
- (16) Hay, P. J.; Thibeault, J. C.; Hoffmann, R. *J. Am. Chem. Soc.* **1975**, *97*, 4884.
- (17) Kirk, M. L.; Shultz, D. A.; Depperman, E. C. *Polyhedron* **2005**, *24*, 2880.
- (18) Kirk, M. L.; Shultz, D. A.; Depperman, E. C.; Brannen, C. L. *J. Am. Chem. Soc.* **2007**, *129*, 1937.
- (19) Kirk, M. L.; Shultz, D. A.; Stasiu, D. E.; Lewis, G. F.; Wang, G. B.; Brannen, C. L.; Sommer, R. D.; Boyle, P. D. *J. Am. Chem. Soc.* **2013**, *135*, 17144.
- (20) Gamelin, D. R.; Kirk, M. L.; Stemmler, T. L.; Pal, S.; Armstrong, W. H.; Pennerhahn, J. E.; Solomon, E. I. *J. Am. Chem. Soc.* **1994**, *116*, 2392.
- (21) Ross, P. K.; Allendorf, M. D.; Solomon, E. I. *J. Am. Chem. Soc.* **1989**, *111*, 4009.
- (22) Tuzcek, F.; Solomon, E. I. *Coord. Chem. Rev.* **2001**, *219*, 1075.
- (23) Tuzcek, F.; Solomon, E. I. *J. Am. Chem. Soc.* **1994**, *116*, 6916.
- (24) Solomon, E. I.; Szilagy, R. K.; George, S. D.; Basumallick, L. *Chem. Rev.* **2004**, *104*, 419.

- (25) *Molecular Magnetism: From Molecular Assemblies to the Devices*; Coronado, E., Delhaes, P., Gatteschi, D., Miller, J. S., Eds.; Kluwer Academic Publishing: Dordrecht, The Netherlands, 1996; Vol. 321.
- (26) Kahn, O. *Molecular Magnetism*; VCH: New York, 1993.
- (27) Chernick, E. T.; Mi, Q. X.; Kelley, R. F.; Weiss, E. A.; Jones, B. A.; Marks, T. J.; Ratner, M. A.; Wasielewski, M. R. *J. Am. Chem. Soc.* **2006**, *128*, 4356.
- (28) Weiss, E. A.; Chernick, E. T.; Wasielewski, M. R. *J. Am. Chem. Soc.* **2004**, *126*, 2326.
- (29) Colvin, M. T.; Carmieli, R.; Miura, T.; Richert, S.; Gardner, D. M.; Smeigh, A. L.; Dyar, S. M.; Conron, S. M.; Ratner, M. A.; Wasielewski, M. R. *J. Phys. Chem. A* **2013**, *117*, 5314.
- (30) Fataftah, M. S.; Zadrozny, J. M.; Coste, S. C.; Graham, M. J.; Rogers, D. M.; Freedman, D. E. *J. Am. Chem. Soc.* **2016**, *138*, 1344.
- (31) Zadrozny, J. M.; Freedman, D. E. *Inorg. Chem.* **2015**, *54*, 12027.
- (32) Yang, J.; Kersi, D. K.; Giles, L. J.; Stein, B. W.; Feng, C. J.; Tichnell, C. R.; Shultz, D. A.; Kirk, M. L. *Inorg. Chem.* **2014**, *53*, 4791.
- (33) Paw, W.; Cummings, S. D.; Mansour, M. A.; Connick, W. B.; Geiger, D. K.; Eisenberg, R. *Coord. Chem. Rev.* **1998**, *171*, 125.
- (34) Cummings, S. D.; Eisenberg, R. *Progress in Inorganic Chemistry: Synthesis, Properties, and Applications* **2003**, *52*, 315.
- (35) Kirk, M. L.; Shultz, D. A.; Stasiw, D. E.; Habel-Rodriguez, D.; Stein, B.; Boyle, P. D. *J. Am. Chem. Soc.* **2013**, *135*, 14713.
- (36) Li, X. H.; Kessissoglou, D. P.; Kirk, M. L.; Bender, C. J.; Pecoraro, V. L. *Inorg. Chem.* **1988**, *27*, 1.
- (37) Baldwin, M. J.; Kampf, J. W.; Kirk, M. L.; Pecoraro, V. L. *Inorg. Chem.* **1995**, *34*, 5252.
- (38) Banci, L.; Bencini, A.; Dei, A.; Gatteschi, D. *Inorg. Chem.* **1983**, *22*, 4018.
- (39) Deumal, M.; Novoa, J. J.; Bearpark, M. J.; Celani, P.; Olivucci, M.; Robb, M. A. *J. Phys. Chem. A* **1998**, *102*, 8404.
- (40) Kirk, M. L.; Shultz, D. A.; Depperman, E. C.; Habel-Rodriguez, D.; Schmidt, R. D. *J. Am. Chem. Soc.* **2012**, *134*, 7812.
- (41) Kirk, M. L.; Shultz, D. A.; Habel-Rodriguez, D.; Schmidt, R. D.; Sullivan, U. *J. Phys. Chem. B* **2010**, *114*, 14712.
- (42) McConnell, H. M.; Chesnut, D. B. *J. Chem. Phys.* **1958**, *28*, 107.
- (43) Scaringe, R. P.; Hodgson, D. J.; Hatfield, W. E. *Mol. Phys.* **1978**, *35*, 701.
- (44) Bencini, A.; Gatteschi, A. *EPR of Exchange Coupled Systems*; Springer-Verlag: New York, 1990.
- (45) Colvin, M. T.; Ricks, A. B.; Scott, A. M.; Co, D. T.; Wasielewski, M. R. *J. Phys. Chem. A* **2012**, *116*, 1923.
- (46) Stein, B. W. *Electronic Structure of the Pyranopterin Dithiolene Cofactor and Radical Reporters of Excited State Interactions*, Ph.D. Dissertation, The University of New Mexico: Albuquerque, NM, 2015.
- (47) Neese, F.; Solomon, E. I. *Inorg. Chem.* **1999**, *38*, 1847.
- (48) Kirk, M.; Peariso, K. *Curr. Opin. Chem. Biol.* **2003**, *7*, 220.
- (49) Heitler, W.; London, F. *Eur. Phys. J. A* **1927**, *44*, 455.
- (50) Best, J.; Sazanovich, I. V.; Adams, H.; Bennett, R. D.; Davies, E. S.; Meijer, A.; Towrie, M.; Tikhomirov, S. A.; Bouganov, O. V.; Ward, M. D.; Weinstein, J. A. *Inorg. Chem.* **2010**, *49*, 10041.
- (51) Kirk, M. L.; Shultz, D. A. *Coord. Chem. Rev.* **2013**, *257*, 218.
- (52) Neese, F. *Wiley Interdiscip. Rev.: Comput. Mol. Sci.* **2012**, *2*, 73.
- (53) Weigend, F.; Ahlrichs, R. *Phys. Chem. Chem. Phys.* **2005**, *7*, 3297.
- (54) Perdew, J. P.; Burke, K.; Ernzerhof, M. *Phys. Rev. Lett.* **1996**, *77*, 3865.
- (55) Angeli, C.; Borini, S.; Cestari, M.; Cimiraglia, R. *J. Chem. Phys.* **2004**, *121*, 4043.
- (56) Angeli, C.; Cimiraglia, R.; Evangelisti, S.; Leininger, T.; Malrieu, J. P. *J. Chem. Phys.* **2001**, *114*, 10252.
- (57) Angeli, C.; Cimiraglia, R.; Malrieu, J. P. *Chem. Phys. Lett.* **2001**, *350*, 297.
- (58) Angeli, C.; Cimiraglia, R.; Malrieu, J. P. *J. Chem. Phys.* **2002**, *117*, 9138.
- (59) Neese, F.; Wennmohs, F.; Hansen, A.; Becker, U. *Chem. Phys.* **2009**, *356*, 98.